INVESTIGATING THE RELATIONSHIP BETWEEN HEAT-INDUCED DNA DAMAGE AND THE SYNAPTONEMAL COMPLEX DURING *C. ELEGANS* SPERMATOGENESIS AND OOGENESIS

by

CAILAN L. FEINGOLD

A THESIS

Presented to the Department of Biology
and the Robert D. Clark Honors College
in partial fulfillment of the requirements for the degree of
Bachelor of Science

May 2021

An Abstract of the Thesis of

Cailan Feingold for the degree of Bachelor of Science
in the Department of Biology to be taken May 2021

Title: Investigating the Relationship between Heat-Induced DNA Damage and the Synaptonemal Complex during *C. elegans* Spermatogenesis and Oogenesis

Approved: _____*Diana E. Libuda, Ph.D.*_____
Primary Thesis Adviser

Approved: ___*Bruce Bowerman, Ph.D.*___
Biology Honors Faculty Representative/Second Reader

Approved: _____*Mark Carey, Ph.D.*_____
Clark Honors College Faculty Representative

Meiosis is utilized by most sexually reproducing organisms to faithfully transmit their genome to the next generation through the production of eggs and sperm. Many aspects of meiosis are sexually dimorphic generating unique differences between spermatogenesis (sperm) and oogenesis (eggs). Spermatogenesis, unlike oogenesis, is sensitive to temperature changes and requires a narrow isotherm of 2-7°C below core body temperature. Sperm exposed to elevated temperatures, both from physiological and environmental conditions, has been linked to increased risks for testicular cancer and male infertility. Although the consequences of increased temperatures on male fertility are well documented, the mechanisms behind this heat-induced male infertility are currently unknown. Using the model system *Caenorhabditis elegans,* we found that spermatocytes display increased DNA damage following exposure to elevated

temperatures, similar to what has been observed in mammals. Further, a critical meiotic chromosome structure, the synaptonemal complex (SC), displays sperm-specific temperature induced premature disassembly during late meiotic prophase I, which correlates with the DNA damage increase following exposure to elevated temperatures. For my honors thesis, I am investigating the relationship between the premature disassembly of the SC and elevated DNA damage in spermatogenesis following heat exposure. By heat shocking *syp-1* mutants, which are unable to assemble the SC under normal conditions, I found sex-specific roles for the SC in influencing heat-induced DNA damage. In spermatocytes, *syp-1* mutants partially suppress the heat-induced DNA damage compared to wild type, thereby suggesting that presence of the SC may be preventing the formation or repair of some heat-induced DNA damage in males. In contrast, *syp-1* mutant oocytes displayed an increase in DNA damage during late prophase I following heat stress. Thus, the SC appears to take on a protective role during oogenesis by suppressing heat-induced DNA damage. Overall, these results uncover an unanticipated role of the SC in its regulation of heat-induced DNA damage that may contribute to sexually dimorphic responses to heat stress during oogenesis and spermatogenesis.

Acknowledgements

I would like to thank Dr. Diana Libuda for providing me with the opportunity to work in her lab and be a part of this fascinating and exciting project. I would also like to thank Dr. Cori Cahoon for her mentorship, her patience as I learned the ropes, and for helping me further develop my love for biology. Together, Cori and Diana have helped to foster my passion for science. Thank you to the entire Libuda Lab for their guidance and support. The lab environment made every day of my research experience enjoyable and I appreciate every member of the lab for their role in my undergraduate project. Because of my experience in the Libuda Lab, I will continue to seek out research opportunities throughout my medical training and practice. Thank you to Dr. Bruce Bowerman for serving on my thesis committee. I would like to thank Dr. Mark Carey for enriching my experience as a Clark Honors College student; you have been a source of support throughout this thesis process and my four years here. A special thank you to my stepparents, Nazy and Guy, for their love, interest, and support throughout my academic career. I am especially thankful for my incredible parents, Lisa and David. Thank you for picking up every phone call to listen to my excitements, my frustrations, my mistakes, and my victories. You inspire me every day to follow my dreams and never give up on myself.

Table of Contents

List of Figures

List of Tables

Introduction

Meiosis

To ensure the survival of a species, it is critical to faithfully pass on the genome from parent to offspring. Organisms that reproduce sexually rely on a specialized form of cell division known as meiosis. Meiosis consists of two rounds of cell divisions (meiosis I and meiosis II), but only one round of DNA replication resulting in the formation of haploid gametes, such as eggs and sperm (Page & Hawley 2003). During meiosis I, homologous chromosomes segregate away from each other, while in meiosis II the sister chromatids segregate away from each other (Figure 1). Errors in this process are known to cause genetic disorders, cancers, and miscarriages (Martin 2008). An abnormal number of chromosomes, or aneuploidy, as a result of errors during meiosis is the leading cause of miscarriages and developmental disabilities (Hassold & Hunt 2001). Whole chromosome missegregation errors during meiosis I are extremely common in human females, accounting for at least 10% of the embryos in human pregnancies (Nagaoka et al. 2012). For women near the end of their reproductive lifespans, the incidence of missegregation errors is closer to 50% (Nagaoka et al. 2012). Further, miscarriages that occur before six weeks showed that 20-40% of preimplantation embryos experience these whole chromosome missegregation errors (Nagaoka et al. 2012). Thus, meiotic errors have severe consequences on human fertility and the physical health of the offspring.

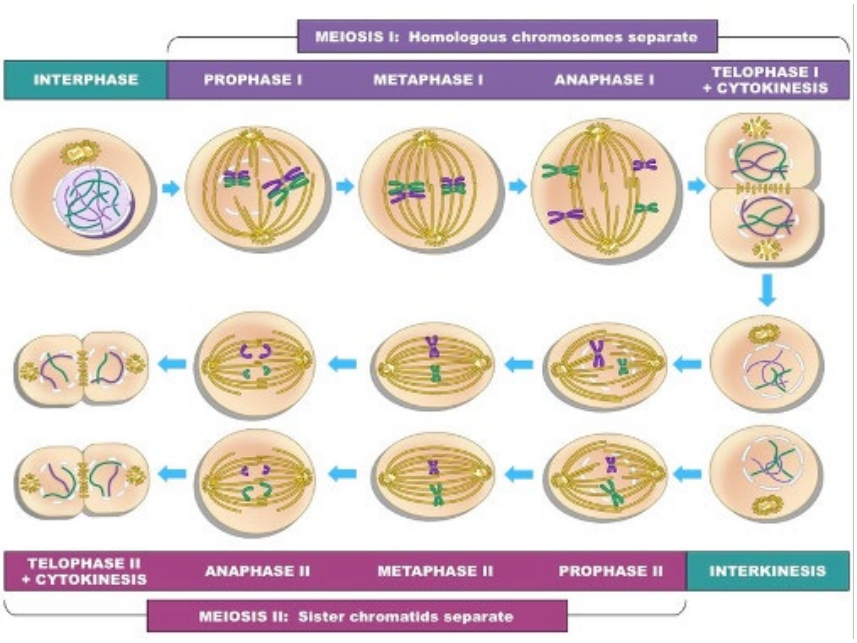

Figure 1: Overview of meiosis

After DNA is replicated during interphase, cells enter meiosis during which they undergo two rounds of divisions. In meiosis I, homologous chromosomes separate, and during meiosis II sister chromatids separate. The products of meiosis are four genetically unique daughter cells with half the number of chromosomes as their parent cells. (Figure adapted from Bioninja)

In order to successfully pass a complete genome on to offspring, meiosis has a number of mechanisms to ensure that chromosome segregation occurs accurately (Roeder 1997, Page & Hawley 2003). First, cells make a series of programmed double strand DNA breaks (DSBs). Of these DSBs, a subset is repaired by homologous recombination, which creates crossovers that physically link homologous chromosomes together. This physical linkage is required in most organisms to orient the homologs away from each other at the first meiotic division ensuring proper chromosome segregation (Page & Hawley 2003). Those DSBs that do not get repaired as crossovers must be accurately repaired by other alternative DNA repair pathways, such as sister chromatid DNA repair. While DSBs are crucial for ensuring homologous recombination

and proper chromosome segregation, it is also essential that they are properly repaired to ensure the genomic integrity is maintained (Lemmens & Tijsterman 2011).

The model organism *C. elegans*

While human female meiosis is quite error-prone at the first division, other organisms have come much closer to perfecting this process. One of these organisms is *Caenorhabditis elegans*, a small, transparent, soil dwelling nematode. The Libuda Lab utilizes this organism to understand multiple aspects of meiosis. *C. elegans* are ideal for biological studies because they are very amenable to genetic manipulation and their transparency is useful for imaging purposes. They can be maintained across a range of temperatures and conditions. *C. elegans* exist in two sexual forms: hermaphrodite and male (Figure 2). Additionally, *C. elegans* share at least 83% protein sequence homology with humans (Lai et al. 2000). Thus, studies done using *C. elegans* helps inform scientists with information that is transferable to humans and other more complex organisms.

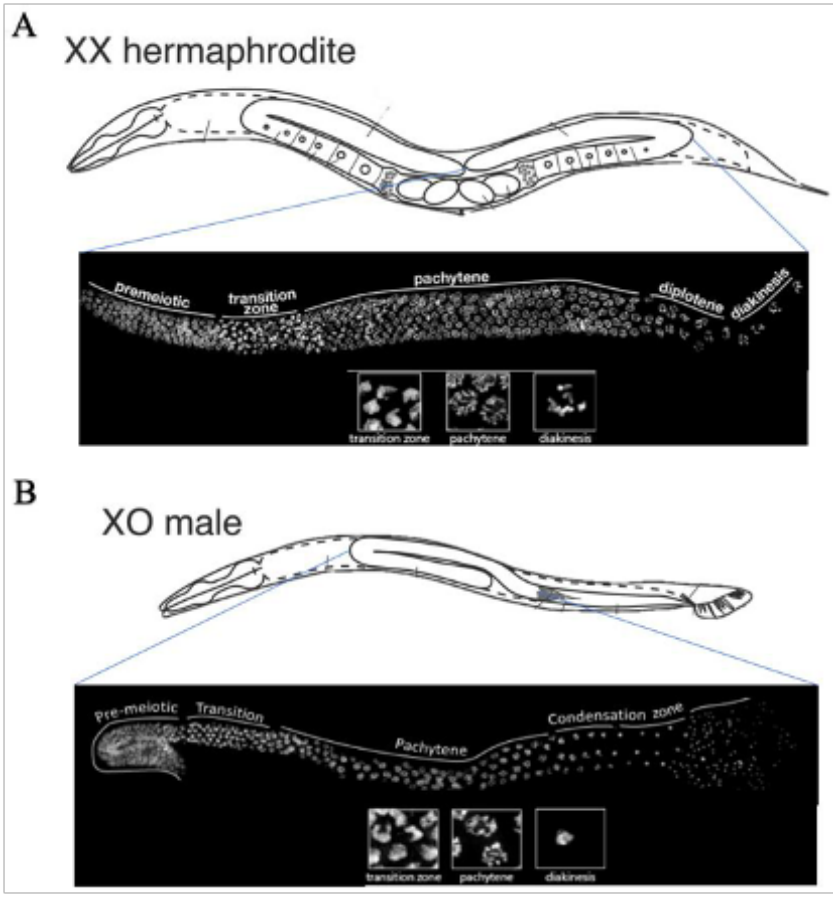

Figure 2: The anatomy of the intact *C. elegans* and dissected germline in males and hermaphrodites

A. Diagram of the anatomy of an intact *C. elegans* hermaphrodite (top) and an extruded, DAPI stained hermaphrodite gonad labeled with the substages of prophase I (below). **B.** Diagram of the anatomy of an intact *C. elegans* male (top) and an extruded, DAPI stained male gonad labeled with the substages of prophase I (below) (Zarkower 2006)

C. elegans are a particularly powerful model system for studying meiosis due to their large gonads and the spatial-temporal organization of the germline (Phillips et al. 2009). This germline organization enables tracking of the germ cell nuclei as they progress from the distal premeiotic tip and through the stages of meiosis while they move within the germline (Lemmens & Tijsterman 2011). Each stage of meiosis is easily identified based on the DNA morphology of the nuclei (Figure 3).

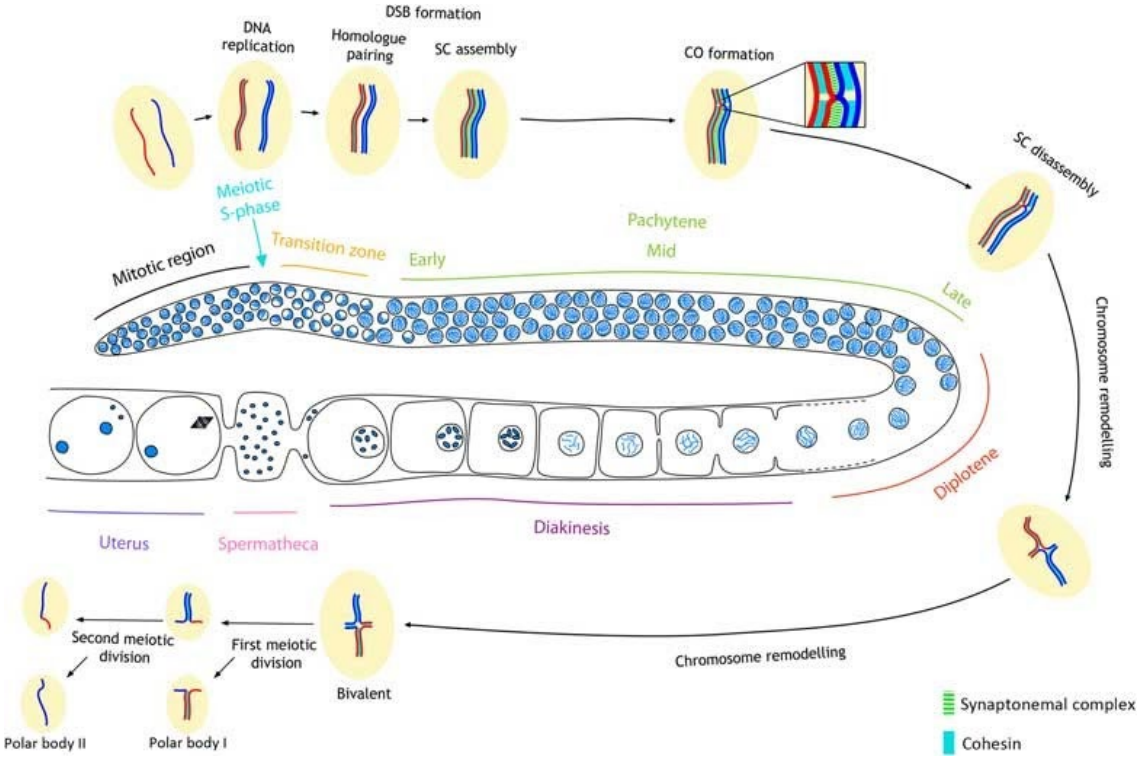

Figure 3: *C. elegans* gonad and meiotic phases overview

Graphic illustrating the spatial-temporal organization of the *C. elegans* germline. Germline nuclei progress from the premeiotic tip to the transition zone and then through pachytene and diplotene before oocytes arrest at diakinesis. (Adapted from Hillers et al. 2017).

At the tip of the germline, germline stem cells undergo mitotic divisions, and this region is referred to as the premeiotic tip. As the nuclei move down the germline, they enter the different stages of meiosis starting with meiotic S phase (meiotic DNA replication). Then, the nuclei move into the transition zone, where homologous chromosomes pair via pairing centers, which are specialized chromosomal regions that mediate the identification of the correct homologous chromosomes (Phillips et al. 2009). Pairing of homologous chromosomes coincides with the construction of the synaptonemal complex (SC), a process known as synapsis (Pattabiraman et al. 2017). The SC is a highly conserved protein complex that assembles between homologous

chromosomes and spans the entire length of the homologs (Cahoon & Hawley 2016). In *C. elegans*, the SC has been shown to play a role in stabilizing pairing associations of chromosomes as meiosis progresses (MacQueen et al. 2002). The SC is a ladder-like structure with lateral elements, central elements, and a central region (Figure 4). The lateral elements run along the chromatin and connect the central region proteins to the chromosomes. The central region proteins span the distance between the homologs and in worms there are 6 proteins that occur in this region: SYP-1, SYP-2, SYP-3, SYP-4, SYP-5 and SYP-6 (MacQueen et al. 2002, Hurlock et al. 2020, Colaiácovo et al. 2003, Smolikov et al. 2007). A subset of proteins within the central region are further defined as central element proteins since they only localize to the middle of the SC and are thought to help stabilize the central region proteins. In worms, only SYP-2 has been identified as a central element protein (Colaiácovo et al. 2003).

After the transition zone, the nuclei enter pachytene, which is defined by having fully synapsed chromosomes and it is during this stage that crossovers are established between homologs (Figure 3). At the end of the transition zone and in early pachytene, DSBs are induced by the conserved endonuclease SPO-11, which breaks the phosphate backbone of the double-strand DNA (Keeney et al. 1997, Dernburg et al. 1998). These breaks progressively get repaired as the nuclei move through the germline (Figure 3). A subset of these DSBs is repaired as crossovers with each chromosome getting one crossover; additionally, the SC is critical for the establishment of crossovers (MacQueen 2002). Those breaks that do not get repaired as crossovers are repaired by alternative repair pathways, such as sister chromatid repair, nonhomologous end-joining, and single-strand annealing (Ranjha et al. 2018). Of these alternative repair

pathways, nonhomologous end-joining and single-strand annealing are more prone to making small DNA errors/deletions during the repair (Clejan et al. 2006).

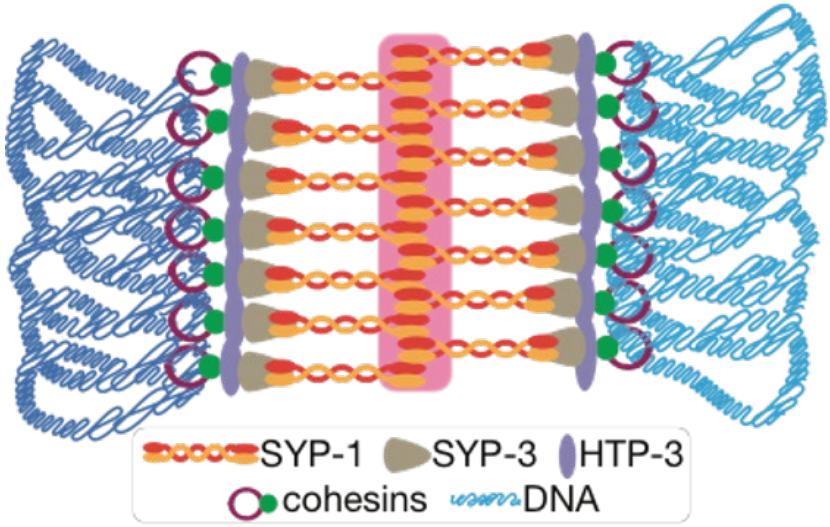

Figure 4: Graphic depicting SC structure

Cartoon figure illustrating the synaptonemal complex, a ladder-like structure made up of a central region and lateral elements. DNA forms chromatin loops and attaches to the lateral elements (Cahoon & Libuda 2019).

At late pachytene and into diplotene and diakinesis, the SC disassembles, and the chromosomes begin to compact into 6 bivalents held together by chiasmata (Villenueve 1994). During diakinesis, oocytes pause their meiotic cycle and will not continue to the next meiotic division until after ovulation and fertilization have occurred. Unlike oocytes, spermatocytes do not arrest at the end of diakinesis and instead continue with the rest of meiosis I and meiosis II generating mature spermatids.

Sexual Dimorphism in Meiosis

Many aspects of meiosis display sexually dimorphic features. The most striking sexually dimorphic feature is the final products of oogenesis and spermatogenesis. Oogenesis produces the largest cell in the body, whereas spermatogenesis produces the

smallest cell in the body. Additionally, the timing of these processes is different. In mammals, oogenesis occurs during fetal development in utero with all the oocytes arresting and being maintained at late prophase I for decades (Huelgas-Morales & Greenstein 2018). Spermatogenesis, on the other hand, occurs throughout the lifespan of the organism. Similar to mammals, *C. elegans* also display sexually dimorphic changes in meiotic timing. In *C. elegans* meiotic prophase I of oogenesis takes 54-60 hours to complete in the adult hermaphrodite, while spermatogenesis prophase I only takes 20-24 hours in the adult male (Jaramillo-Lambert et al. 2007).

The SC also exhibits sexual dimorphism. The organization of the axial elements of chromosome structure has been demonstrated to vary between sexes (Cahoon & Libuda 2019). The SC assembles upon these sexually dimorphic axial elements and as a result many lateral element proteins exhibit sex-specific changes. In mice, it has been shown that mutants in two lateral element proteins (SCP3, SYCP2) cause a complete failure of SC assembly in males, but only a partial SC assembly defect in females (Yuan et al. 2000; Yang et al. 2006).

Spermatogenesis, unlike oogenesis and other biological processes, must occur 2-7°C below core body temperature and exposing spermatocytes to elevated temperatures has been linked to male infertility and cancer (Rao et al. 2015, Kim et al. 2013, Perez-Crespo et al. 2008). Around one out of six couples worldwide face infertility issues and about half of these cases are the consequence of defects in male-specific factors (Schlegel 2009). Previous studies have shown that elevated testicular temperatures cause an increase in DNA damage in mammals and *C. elegans* (Perez-Crespo et al. 2008, Kurhanewicz et al. 2020). Additionally, the Libuda Lab has found

that the SC appears to disassemble prematurely in only *C. elegans* spermatogenesis following heat stress. However, the relationship between heat-induced increases in DNA damage and premature disassembly of the SC remains unclear.

My research focused on understanding whether the SC regulates the heat-induced DNA damage in spermatocytes. I hypothesized that the premature breakdown of the SC causes the elevated levels of DNA damage in spermatocytes following heat stress. To test this, I utilized *syp-1* mutants, which lack the SC, and exposed them to heat stress before quantifying DNA damage levels. In males, loss of the SC partially suppressed the heat-induced DNA damage when compared to wild type, suggesting that the presence of the SC may be hindering repair of heat-induced DSBs in spermatocytes. In hermaphrodites, I found a protective role against heat-induced DNA damage, as *syp-1* oocytes displayed an increase in heat-induced DSBs compared with wild type. Together, these findings uncover a sexually dimorphic role for the SC in its relationship with heat-induced DNA damage.

Methods

C. elegans strains

C. elegans strains were kept at either 15°C or 20°C. They were maintained on *E. coli* OP50 lawns grown on Nematode Growth Medium (NGM) petri plates. OP50 is an uracil-deficient *E. coli* mutant, which prevents overgrowth of the lawn (Brenner, 1974). For wild type strains (N2), mating consisted of a ratio of 1:3 hermaphrodites to males.

Strain Name	Strain Genotype
N2	Wild type
AV761	GFP::COSA-1 II; spo-11(me44) IV/ nT1[qIs51]
DLW91	syp-1(me17) V/nT1 [unc-?(n754) let-? qIs50] (IV;V).
DLW90	meIs8[unc-119(+) pie-1promoter::gfp::cosa-1]/+ II; spo-11(ok79) IV; syp-1(me17) V/nT1[unc-?(n754) let-? qIs50] (IV;V).

Table 1: *C. elegans* strains used in this study and corresponding genotypes

Immunohistochemistry

For each strain, ~40 L4 males and ~40 L4 hermaphrodites were transferred to 2 new NGM + OP50 plates and kept at 20°C overnight. One plate became the no heat-shock (NOHS) group and the other became the heat-shock (HS) group. The NOHS group was kept 20°C while the HS group underwent heat-sock. The HS group was incubated at 34°C for 2 hours, followed by a 1-hour recovery period at 20°C before they underwent dissection.

For dissection, the worms were transferred to a 30 µL droplet of a solution containing 1x egg buffer and 0.1% Tween20 on a 22 x 22 mm coverslip. A 23G needle was used to make a cut through the pharynx of the worm while the worm swam in the egg buffer. The movement of the worm with the released pressure of the cut caused the gonad to extrude. Dissection of each treatment group did not exceed 30 minutes. 15 µL of the egg buffer with the dissected gonads was transferred to a new 22x22 coverslip and 15 µL of 2% paraformaldehyde was added to fix the gonads to the slide. The paraformaldehyde and egg buffer were carefully mixed on the new coverslip by pipetting up and down before removing 20 µL of the solutions, without disturbing the gonads. A Superfrost Plus slide was immediately placed on top of the coverslip and any bubbles between the slide and the coverslip were removed. After 5 minutes the coverslip and slide were submerged in liquid Nitrogen for one minute. Upon removal from the liquid Nitrogen, the coverslip was immediately flicked off of the Superfrost Plus slide, tearing off the worm cuticle. The slide was then placed in -20°C methanol for one minute, followed by 3 immersions in 1x PBST. The slide was then washed in 1x PBST 3 more times in 10-minute increments before being blocked in 0.7% bovine serum albumin (BSA) in PBST for 1 hour.

After 1 hour in block, 50 µL of diluted primary antibodies were added to each slide and covered with a parafilm slice, which helped ensure distribution of the antibody. These slides were incubated in a humidifying chamber at room temperature overnight. The next morning, slides were washed 3 times in 1x PBST for 10 minutes each. 50 µL of secondary antibody was then added and the slide was covered again with parafilm. The slides were incubated for two hours in a dark humidifying chamber at

room temperature. After this incubation, the slides were washed 3 times in 1x PBST for ten minutes each in the dark.

After being washed in the dark, 50 µL of 2µg/mL DAPI diluted in water were added to each slide. The slides were then covered again by parafilm and incubated in the dark for 5 minutes. The slides were then washed in 1x PBST for 10 minutes in the dark. We used 15 µL Vectashield to seal the 20 x 40 mm coverslip over the gonads. We removed any bubbles that had formed between the coverslip and the slide before sealing the coverslip using clear nail polish. The slides were stored in the dark at 4°C.

Microscopy

All imaging was done using the Applied Precision DeltaVision Elite High-Resolution Microscope. Images were taken using the 60x objective with an oil immersion of 0.514 refraction index. Using the softWoRx software, imaging times and transmission percentages were determined for each color channel. The softWoRx software was also used to determine the thickness of each individual gonad; images were then acquired as Z stacks with 0.2mm intervals. Deconvolution was performed by the softWoRx software over 15 cycles. Figure images were generated by max intensity Z projections and adjusted for both brightness and contrast to reduce background signal using the image analysis software FIJI.

Quantitative DSBs

To analyze the data as a function of position along the germline, I utilized the Gonad Analysis Pipeline, which was constructed within the Libuda Lab by using image quantification software and custom scripts in MATLAB and R (Toraason et al. 2021).

Briefly, DeltaVision images were stitched using the FIJI plugin Stitcher (Preibisch et al. 2009) and the 3D software Imaris was used to segment nuclei and count RAD-51 foci per nucleus. Then, a custom R script was used to analyze RAD-51 foci along the entire germline. This program normalized the germline lengths on a scale from 0 to 1 where 0 symbolizes the beginning of the transition zone and 1 symbolizes the end of late pachytene. This program also distributed the RAD-51 foci levels across the normalized germline. Data was sorted into five equal-sized bins based on germline position; each bin represents one-fifth of the normalized germline length. Once the data was sorted into these five bins, the average RAD-51 foci per nucleus was calculated for each bin.

Statistics

RAD-51 foci per nucleus counts were analyzed using a Mann-Whitney statistical test to compare two groups at a time with the significance level set at 0.05.

Results

syp-1 mutant hermaphrodites display increased DNA damage following heat stress

To investigate the effects of the SC on heat-induced DNA damage, I used wild type worms and *syp-1* null mutants. SYP-1 is a central region protein of the SC, and *syp-1* null mutants cause a complete loss of the SC structure (MacQueen et al. 2002). In hermaphrodites, previous studies have shown that *syp-1* mutants have many additional meiotic defects due to the lack of the SC including defects in homologous chromosome pairing, chromosome organization, and recombination (MacQueen et al. 2002). These defects trigger checkpoint delays within the germline that cause an extended transition zone and increased DSBs as the cells attempt to synapse and establish a crossover (Bhalla & Dernburg 2005, Bohr et al. 2016). Eventually, the checkpoint delays in *syp-1* mutants are alleviated by allowing the cells to proceed through a very short pachytene stage and finish meiosis regardless of the meiotic defects (MacQueen et al. 2002).

To determine the number of DSBs, I performed immunofluorescence staining for the recombinase protein RAD-51, which marks DSBs undergoing DNA repair using homologous recombination. Using a combination of the 3D image analysis software and a custom algorithm, I quantified the number of RAD-51 foci per nucleus along the germline from the start of the transition zone to the end of late pachytene in worms exposed to 34ºC (heat shock) and worms not exposed to 34ºC (no heat shock) (see methods, Toraason et al. 2021). To compare the germline distributions of RAD-51 foci between wild type and *syp-1* mutants, the germline lengths were normalized with 0 indicating the start of the transition zone and 1 indicating the end of late pachytene. I

then sorted the data into five equal-sized bins based on germline position, with each bin representing one-fifth of the normalized germline length to obtain the average RAD-51 foci per bin. This normalization and grouping of the data allowed for direct comparison between wildtype and *syp-1* germlines regardless of the morphological changes to the germline created by the *syp-1* mutant.

From this analysis, I recapitulated the previously published results from the Libuda Lab showing that upon heat stress, wild type hermaphrodites did not exhibit an increase in DNA damage (Kurhanewicz et al. 2021) (Figure 5). Wild type hermaphrodites not exposed to heat stress displayed the largest increase in DSBs within bin 2 (wild type no heat stress average number of RAD-51: 2.9 ± SD 2.4) (SD = standard deviation), and then the foci number progressively decreased through bins 3 to 5 (average number of RAD-51: bin 3=1.7 ± SD1.8, bin 4= 0.6 ± SD1.1, bin 5=0.4 ± SD0.7) indicating that all these DSBs are in the process of being repaired by the end of late pachytene (Figure 5B). Heat stressed wild type hermaphrodites displayed a very similar pattern of RAD-51 foci (wild type heat stress average RAD-51 foci: bin 1=2.4 ± SD3.9, bin 2=3.1 ± SD4.1, bin 3=1.3 ± SD1.8, bin 4=0.3 ± SD0.7, bin 5=0.4 ± SD1.6) (Figure 5B). Thus, wild type hermaphrodites did not exhibit changes in RAD-51 foci follow heat stress.

To investigate how loss of the SC affects heat-induced DNA damage, *syp-1* null mutants were heat shocked and RAD-51 was quantified as described above. *syp-1* hermaphrodites not exposed to heat stress exhibited higher RAD-51 levels across the germline than the wild type worms not exposed to heat stress ($p<0.001$ for bins 1, 3, 4, and 5, Mann Whitney). Additionally, unlike not heat stressed wild type hermaphrodites,

not heat stressed *syp-1* hermaphrodites did not display a progressive decrease in RAD-51 foci towards the end of pachytene in bin 5 (*syp-1* average RAD-51 foci: bin 4=5.3 ± SD3.1, bin 5=4.4 ± SD2.9; wild type average RAD-51 foci: bin 4 =0.6 ± SD1.1, bin5=0.4 ± SD0.7; $p<0.05$ for bins 3-5, Mann Whitney). Both the observed slight increase in baseline levels of RAD-51 foci and the persisting foci into late pachytene have been previously shown to be hallmarks of SC defect mutants (MacQueen et al. 2002).

Unlike heat stressed wild type hermaphrodites, heat stressed *syp-1* hermaphrodites did experience increases in DNA damage levels. Across the entire germline, the amount of RAD-51 foci progressively increased, like with the *syp-1* hermaphrodites that did not undergo heat stress, from bins 1 to 4 (*syp-1* heat stress: bin 1=3.8 ± SD6.5, bin 2=6.6 ± SD8.8, bin 3=5.4 ± SD9.1, bin 4=9.1 ± SD13.3; *syp-1* no heat stress: bin 1=0.1 ± SD0.5, bin 2=2.2 ± SD1.6, bin 3=5.3 ± SD 2.6, bin 4=5.3 ± SD3.1; $p<0.05$ bins 1, 3, & 5, Mann Whitney) (Figure 5B). However, heat stressed *syp-1* hermaphrodites displayed the most significant increase in RAD-51 foci in bin 5 (*syp-1* heat stress bin 5=18.6 ± SD21; wild type heat stress bin 5=0.4 ± SD1.6; *syp-1* no heat stress bin 5=4.4 ± SD2.9) (Figure 5B). The increase in DNA damage seen in *syp-1* oocytes in bin 5 is significant compared with both heat stressed wild type oocytes and not heat stressed *syp-1* oocytes (*syp-1* heat stress vs. *syp-1* no heat stress: $p=0.039$, Mann Whitney; *syp-1* heat stress vs. wild type heat stress: $p<0.00001$, Mann Whitney). While these *syp-1* mutants have higher baseline level of DSBs, the observed increases in RAD-51 foci within heat stressed *syp-1* mutants in bin 5 is over four times higher

than the baseline of *syp-1* mutants not exposed to heat stress. Therefore, in hermaphrodites the SC appears to suppress or prevent heat-induced DNA damage.

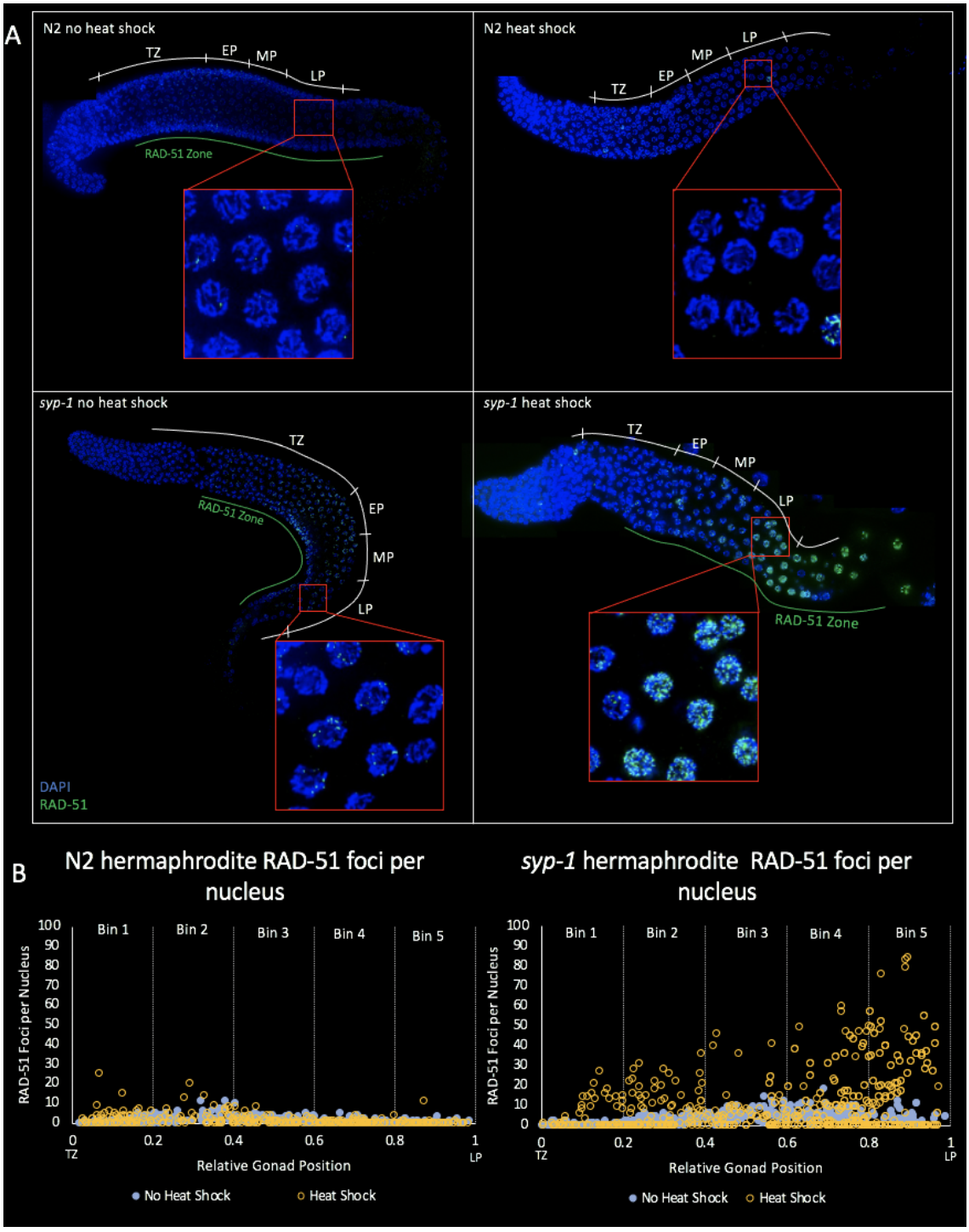

Figure 5: Heat stress causes elevated DNA damage in *syp-1* null mutants during oogenesis

(A) Immunofluorescence images of whole gonads featuring recombinase RAD-51 marking sites of DNA damage (green) and DAPI marking the DNA (blue). Windows featuring a zoomed in view to late pachytene are boxed in red. Images of wild type adult hermaphrodites and *syp-1* null mutant hermaphrodites both with and without heat shock are included. The RAD-51 zone is marked by a solid green line. The stages of meiotic prophase I are marked with a white line.

(B) Scatterplots illustrating the quantification of RAD-51 foci per nucleus. The x axis represents the normalized length of the germline with 0 representing the beginning the of the transition zone and 1 representing the end of late pachytene. The y axis is the number of RAD-51 foci per nucleus, ranging from 0 foci to 100 foci. Data from the no heat shock group is represented by the solid blue dots, while data from the heat shock group is represented by the open yellow dots. Wild type (N2) hermaphrodites are represented by the scatterplot to the left and *syp-1* null hermaphrodites are represented by the scatterplot to the left. N2 hermaphrodite no HS: n=3, N2 hermaphrodite HS: n=3, *syp-1* hermaphrodite no HS: n=3, *syp-1* hermaphrodite HS: n=3.

Average RAD-51 foci per nucleus of wild type no heat shock hermaphrodites: bin 1=0.8±SD1.1, bin 2= 2.9±SD2.4, bin 3=1.7±SD1.8, bin 4=0.6±SD1.1, bin 5=0.4±SD0.7. Average RAD-51 foci per nucleus of wild type heat shock hermaphrodites: bin 1=2.4±SD3.9, bin 2=3.1±SD4.1, bin 3=1.3±SD1.8, bin 4=0.3±SD0.7, bin 5= 0.4±SD1.6. Average RAD-51 foci per nucleus of *syp-1* no heat stress hermaphrodite: bin 1=0.2±SD0.5, bin 2=2.2±SD1.6, bin 3=5.3±SD2.9, bin 4=5.3±SD3.1, bin 5=4.4±SD2.9. Average RAD-51 foci per nucleus *syp-1* heat stress hermaphrodites: bin 1=3.8±SD6.5, bin 2=6.6±SD8.8, bin 3=5.4±SD9.1, bin 4-9.1±SD13.3, bin 5=18.6±SD21,

Oocytes lacking the SC experience an increase in SPO-11 independent DNA damage in late pachytene following heat stress.

The elevated levels of baseline SPO-11 induced DSBs in a *syp-1* mutant makes it difficult to determine the magnitude by which heat-induced DNA damage increased in hermaphrodites lacking the SC. To circumvent this issue, we removed all meiotic DSBs using a *spo-11* null mutant, which eliminates the formation of meiotic DSBs both in *spo-11* single mutants and *spo-11; syp-1* double mutants (Cahoon et al. 2019, Dernburg et al. 1998, Colaiácovo et al. 2003). By comparing these mutants, I observe how loss of the SC affects heat-induced DNA damage without the higher baseline levels of RAD-51 foci in the background.

The *spo-11* hermaphrodites that were not exposed to heat stress exhibited very low levels of DNA damage, as expected due to loss of endogenous meiotic DSBs (Figure 6B). Upon heat stress, DNA damage levels in *spo-11* hermaphrodites did not significantly change ($p>0.05$ for all bins, Mann Whitney) (Figure 6). This result indicates that in hermaphrodites, when the SC is present, we do not see the same SPO-11 independent DNA damage following heat stress that we see in males. This finding corroborates research out of the Libuda lab that reveals that only males experience SPO-11 independent DNA damage following heat stress (Kurhanewicz et al. 2021).

Next, we examined the effect of heat stress on *spo-11; syp-1* double mutants to understand how a loss of the SC in this background influences heat-induced DNA damage. The not heat stressed *spo-11; syp-1* hermaphrodites displayed low levels of average RAD-51 foci, similar to the heat stressed and not heat stressed *spo-11* single mutants (Figure 6). Surprisingly, upon heat stress exposure, the *spo-11; syp-1* double

mutant hermaphrodites exhibited a significant increase in RAD-51 foci within bins 3-5, which roughly corresponds to the mid to late pachytene regions ($p<0.05$ for bins 3-5, Mann Whitney) (Figure 6). The largest increase occurred within bin 5, which had an average RAD-51 foci of 0.1 ± SD0.5 foci in not heat stressed *syp-1; spo-11* compared to 3.2 ± SD8.3 average RAD-51 foci in heat stressed *syp-1; spo-11* ($p=0.0014$, Mann Whitney) (Figure 6B). This result suggests that when the SC is absent, hermaphrodites do experience an increase in SPO-11 independent heat-induced DNA damage towards the end of pachytene.

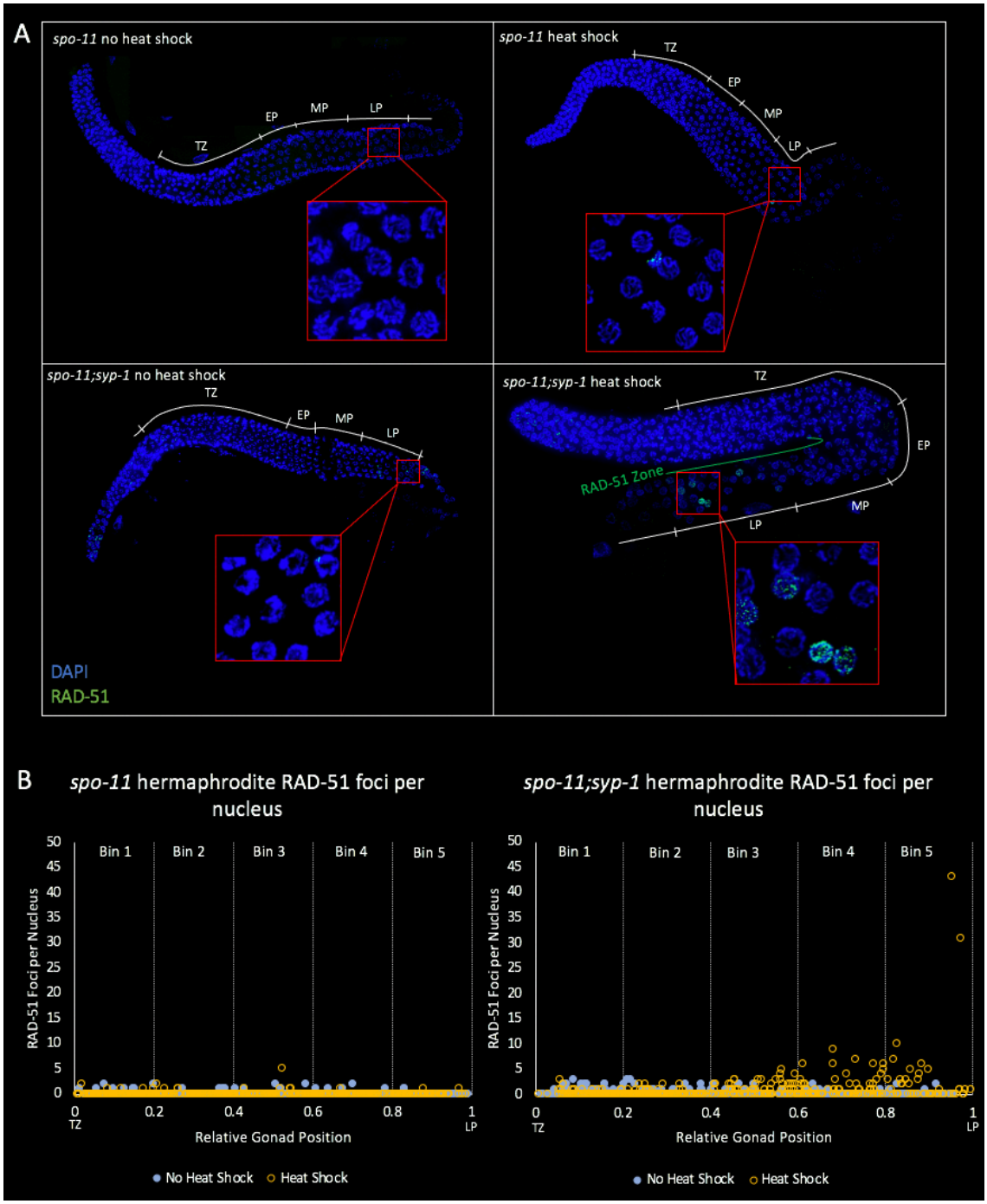

Figure 6: Absence of the SC in oocytes promotes heat-induced DNA damage in late pachytene.

(A)Immunofluorescence images of whole gonads featuring recombinase RAD-51 marking sites of DNA damage (green) and DAPI marking the DNA (blue). Windows featuring a zoomed in view to late pachytene are boxed in red. Images of *spo-11* null hermaphrodites and *spo-11; syp-1* double mutant hermaphrodites both with and without heat shock are included. The RAD-51 zone is marked by a solid green line. The stages of meiotic prophase I are marked with a white line.

(B) Scatterplots illustrating the quantification of RAD-51 foci per nucleus. The x axis represents the normalized length of the germline with 0 representing the beginning the of the transition zone and 1 representing the end of late pachytene. The y axis is the number of RAD-51 foci per nucleus, ranging from 0 foci to 100 foci. Data from the no heat shock group is represented by the solid blue dots, while data from the heat shock group is represented by the open yellow dots. *spo-11* null hermaphrodites are represented by the scatterplot to the left and *spo-11; syp-1* double mutant hermaphrodites are represented by the scatterplot to the left. *spo-11* hermaphrodite no HS: n=4, *spo-11* hermaphrodite HS: n=3, *spo-11; syp-1* hermaphrodite no HS: n=3, *spo-11; syp-1* hermaphrodite HS: n=3.

Average RAD-51 foci per nucleus of no heat stress *spo-11* hermaphrodite: bin 1=0.1±SD0.3, bin 2=0.1±SD0.3, bin 3=0.0±SD0.2, bin 4=0.0±SD0.2, bin 5=0.0±SD0.1. Average RAD-51 foci per nucleus of heat stress *spo-11* hermaphrodite: bin 1=0.1±SD0.3, bin 2=0.1±SD0.3, bin 3=0.1±SD0.6, bin 4=0.0±SD0.1, bin 5=0.0±SD0.2. Average RAD-51 foci per nucleus of no heat stress *spo-11; syp-1* hermaphrodite: bin 1=0.3±SD0.6, bin 2=0.3±SD0.7, bin 3=0.2±SD0.5, bin 4=0.1±SD0.4, bin 5=0.1±SD0.5. Average RAD-51 foci per nucleus of heat stress *spo-11; syp-1* hermaphrodite: bin 1=0.2±SD0.5, bin 2=0.2±SD0.5, bin 3=0.9±SD1.2, bin 4=1.1±SD1.9, bin 5=3.2±SD8.3.

In order to understand if this significant increase is a result of the loss of the SC during heat stress, I compared data from heat stressed *spo-11; syp-1* hermaphrodites with data from heat stressed *spo-11* hermaphrodites. This comparison allows me to consider a statistical difference with only one variable at hand: presence or absence of the SC. I found that heat stressed *spo-11; syp-1* hermaphrodites had significantly more RAD-51 foci within bins 3-5 than heat stressed *spo-11* hermaphrodites ($p<0.0001$ for

bins 3-5, Mann Whitney) (Figure 6B). Thus, hermaphrodites experience an increase in DNA damage following heat stress in the mid to late pachytene regions when the SC is absent. This result suggests that the SC may have a protective role against heat-induced DNA damage in hermaphrodites.

syp-1 mutant spermatocytes have increased DNA damage following heat stress

To investigate the role of the SC in heat-induced DNA damage during spermatogenesis, we performed the same heat stress experiments and subsequent RAD-51 quantification in wild type and *syp-1* males (see methods). As was shown previously by the Libuda lab, wild type males exhibit significantly higher numbers of RAD-51 foci per nucleus following heat stress (Kurhanewicz et al. 2020). Notably, after heat stress, the RAD-51 foci number of wild type males significantly increased throughout the germline with the peak number of foci occurring in bin 5 (wild type heat stress average RAD-51 foci bin 5=31.8 ± SD16; wild type no heat stress bin 5=0.1 ± 0.4; $p<0.00001$ for bins 1-5, Mann Whitney) (Figure 6B). The not heat stressed wild type males exhibited their highest levels of DNA damage in bin 2 (Average RAD-51 foci: bin 2=4.3 ± SD3.6) and experienced a decrease in DNA damage following bin 2 (Average RAD-51 foci: bin 3=1.9 ± SD2.3, bin 4=0.5 ± SD1.0, bin 5=0.9 ± SD0.4) indicating that DSBs are being repaired as they progress through the germline (Figure 6B).

We then studied the effects of heat stress on *syp-1* males using the same heat stress experiment and RAD-51 quantification protocol (see Methods). *syp-1* males that did not undergo heat stress displayed a significant increase in RAD-51 foci in bins 1, 3, and 4 compared with not heat stressed wild type males (*syp-1* no heat stress: bin 1=2.8 ± SD2.6, bin 3=4.0 ± SD3.3, bin 4=0.8 ± SD1.2; wild type no heat stress: bin 1=2.5 ±

SD.3.6, bin 3=1.9 ± SD2.3, bin 4=0.5 ± SD1.1; bin 1 p-value=0.025, bin 3 p-value=0.00004, bin 4 p-value=0.0223, Mann Whitney) (Figure 7B). Surprisingly, *syp-1* males do not experience significantly higher DNA damage levels in bin 5 (*syp-1* no heat stress bin 5=2.8 ± SD2.6; wild type no heat stress bin 5=2.5 ± SD3.6, p-value=0.169, Mann Whitney). This result is an unexpected deviation from hermaphrodite findings, where *syp-1* mutants experience significantly higher levels of DNA damage that persist into bin 5 (Figure 5B). Unlike *syp-1* hermaphrodites, males lacking the SC display DNA damage levels similar to their wild type counterparts in the section of the germline that roughly corresponds to late pachytene.

Following heat stress, *syp-1* males exhibited higher levels of DNA damage that increased progressively from bins 1 to 4 (*syp-1* male heat stress: bin 1=19.4 ± SD12.7, bin 2=25 ± SD18.7, bin 3=26 ± SD19.1, bin 4=37.5 ± SD26.7; $p<0.00001$ for bins 1-4, Mann Whitney) (Figure 7B). Like the not heat stressed *syp-1* males, the heat stressed *syp-1* males also exhibited a drop off in DNA damage levels from bin 4 to bin 5 (*syp-1* male heat stress bin 5=31.2 ± SD 19.3), however bin 5 is still significantly higher following heat stress than in not heat stressed *syp-1* males ($p<0.00001$, Mann Whitney) (Figure 7B). Therefore, males still experience an increase in DNA damage levels following heat stress throughout the gonad, even in the absence of the SC.

The data also indicates that *syp-1* males may experience a slight increase in DNA damage following heat stress compared with heat stressed wild type males. For example, upon comparing the DNA damage of bin 2 of wild type heat stressed males (average RAD-51 foci: bin 2=17.6 ± SD13.2) with that of *syp-1* heat stressed males (average RAD-51 foci: bin 2=25 ± SD18.7) we see a significant increase (bin 2

p=0.00776, Mann Whitney) (Figure 7B). The increase in DNA damage seen in heat stressed *syp-1* males compared with wild type heat stressed males, however, was not significant in bins 1 and 3-5 ($p>0.05$ for bins 1, 3, 4, & 5) (Figure 7B). This result preliminarily suggests that a loss of the SC may cause a more exaggerated increase in DNA damage following heat stress in spermatocytes, at least in the transition zone.

Although these *syp-1* mutants are known to have higher baseline levels of DSBs, the average RAD-51 foci within heat stressed *syp-1* males in bin 5 is over 15-fold higher than baseline RAD-51 foci in not heat stressed *syp-1* males (*syp-1* heat stress bin 5=31.2 ± SD 19.3, *syp-1* no heat stress bin 5=0.2 ± SD0.5) (Figure 7B). Therefore, I can reason that the known baseline increase in DSBs in *syp-1* mutants does not negate the significant increase in DNA damage seen in *syp-1* males following heat stress.

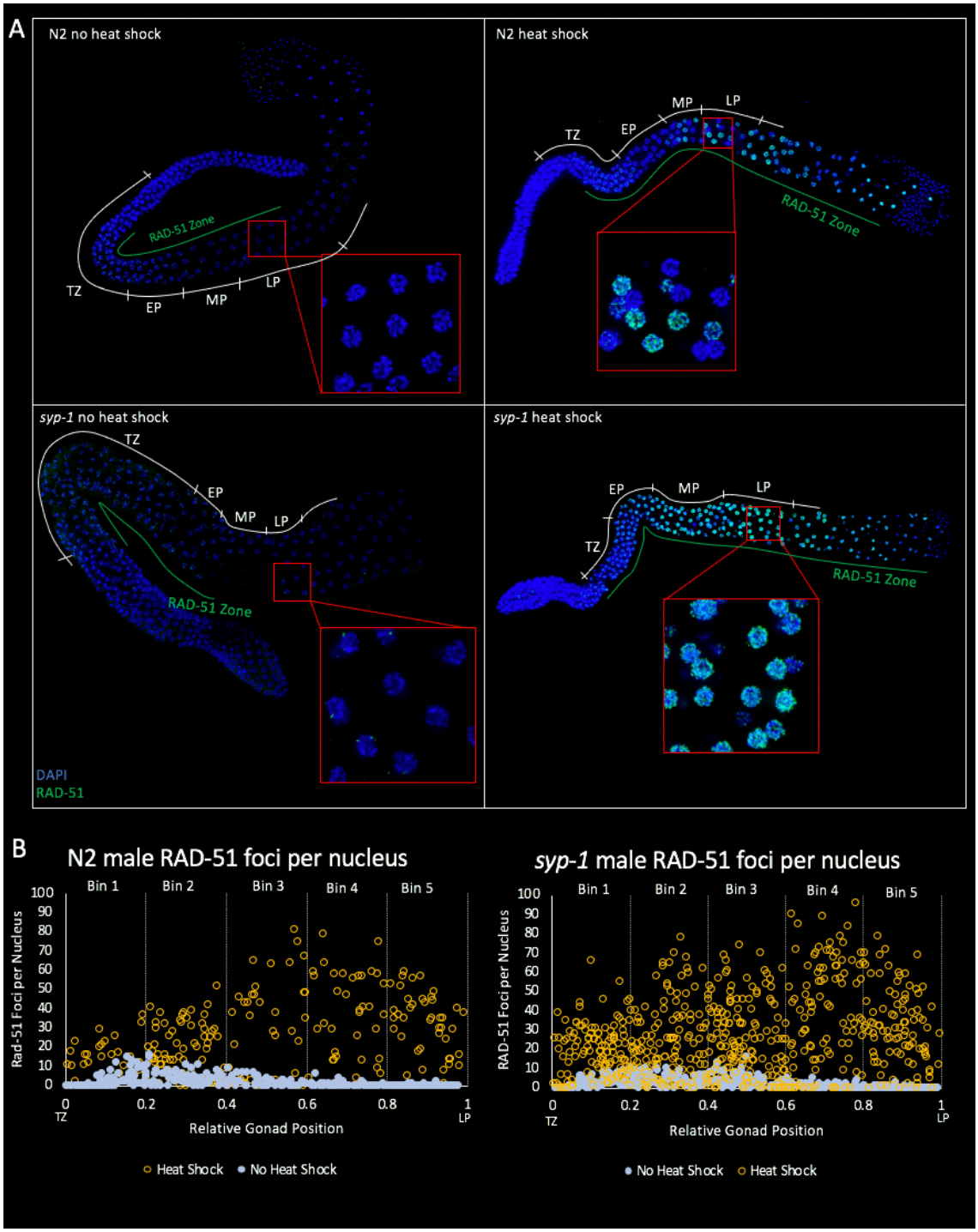

Figure 7: DNA damage is elevated in *syp-1* spermatocytes following heat stress

(A)Immunofluorescence images of whole gonads featuring recombinase RAD-51 marking sites of DNA damage (green) and DAPI marking the DNA (blue). Windows featuring a zoomed in view to late pachytene are boxed in red. Images of wild type adult males and *syp-1* null mutant males both with and without heat shock are included. The RAD-51 zone is marked by a solid green line. The stages of meiotic prophase I are marked with a white line.

(B) Scatterplots illustrating the quantification of RAD-51 foci per nucleus. The x axis represents the normalized length of the germline with 0 representing the beginning the of the transition zone and 1 representing the end of late pachytene. The y axis is the number of RAD-51 foci per nucleus, ranging from 0 foci to 100 foci. Data from the no heat shock group is represented by the solid blue dots, while data from the heat shock group is represented by the open yellow dots. Wild type (N2) males are represented by the scatterplot to the left and *syp-1* null males are represented by the scatterplot to the left. N2 male no HS: n=3, N2 male HS: n=3, *syp-1* male no HS: n=3, *syp-1* male HS: n=6.

Average RAD-51 foci per nucleus of wild type no heat stress males: bin 1=2.5±SD3.6, bin 2=4.3±SD3.6, bin 3=1.9±SD2.3, bin 4=0.5±SD1.1, bin 5=0.1±SD0.3. Average RAD-51 foci per nucleus of wild type heat stress males: bin 1=16.4±SD8.6, bin 2=17.5±SD13.2, bin 3=26.7±SD24.8, bin 4=35.2±SD22.6, bin 5=31.8±SD16.1. Average RAD-51 foci per nucleus of *syp-1* no heat stress males: bin 1=2.8±SD2.6, bin 2=4.4±SD3.0, bin 3=4.0±SD3.3, bin 4=0.8±SD1.2, bin 5=0.2±SD0.5. Average RAD-51 foci per nucleus of *syp-1* heat stress males: bin 1=19.4±SD12.7, bin 2=25±SD18.7, bin 3=26±SD19.1, bin 4=37.5±SD26.7, bin 5=31.2±SD19.3.

spo-11; syp-1 **males experience a suppression of heat-induced DNA damage compared with** ***spo-11*** **males.**

While the elevated baseline levels of SPO-11 induced DNA damage in *syp-1* mutants do not invalidate the increase in DNA damage following heat stress in *syp-1* males, this baseline elevation does make it more difficult to discern the magnitude by which the DNA damage increased. For this reason, I again used *spo-11* single and *spo-11; syp-1* double mutants where the elevated baseline levels of SPO-11 induced DNA

damage are absent (Cahoon et al. 2019, Dernburg et al. 1998, Colaiácovo et al. 2003). Additionally, previous research from the Libuda Lab has found that heat-induced DNA damage in spermatocytes is SPO-11 independent (Kurhanewicz et al. 2020). Therefore, using the *spo-11; syp-1* mutant, I can determine if all of the heat-induced damage in *syp-1* males is occurring independent of SPO-11(Kurhanewicz et al. 2020).

RAD-51 immunofluorescence assays and RAD-51 quantification were conducted on *spo-11* males and *spo-11; syp-1* double mutant males that had undergone heat stress and those that had not (see methods). The *spo-11* males that did not undergo heat stress exhibited very low levels of DNA damage; no bin held an average number of RAD-51 foci higher than 0.1 (Figure 8B). This result was expected, as we know that *spo-11* mutants do not experience endogenous breaks and without heat stress we would not anticipate an exogenous source of DNA damage. The *spo-11* null males that did undergo heat stress experienced significantly higher levels of RAD-51 foci throughout the normalized germline ($p<0.00001$ for all bins, Mann Whitney) (Figure 8). Average RAD-51 foci in *spo-11* heat stressed males were the highest throughout bins 3-5 (*spo-11* heat stress: bin 3=34.4 ± SD21.6, bin 4=34.9 ± SD21.6, bin 5=34.1 ± SD17.2; *spo-11* no heat stress: bin 3=0.1 ± SD0.3, bin 4=0.1 ± SD0.1, bin 5=0.1 ± SD0.3; $p<0.00001$ for bins 3-5, Mann Whitney) (Figure 8B). This data corroborates the findings of Kurhanewicz et al. 2020, as we see that *spo-11* null males still experience significant increases in DNA damage following heat stress.

To determine if the SC influences DNA damage independent of SPO-11, we ran the same heat stress experiments on the *spo-11; syp-1* double mutant males. The not heat stressed *spo-11; syp-1* males exhibited extremely low levels of DNA damage,

similar to not heat stressed *spo-11* males (Figure 8B). Upon experiencing heat stress, the *spo-11; syp-1* males displayed an increase in RAD-51 foci that was significant for the entirety of the normalized germline ($p<0.00001$ for all bins, Mann Whitney) (Figure 8). The greatest increase seen in heat stressed *spo-11; syp-1* males was in bin 5, which roughly correlates with the late pachytene region of the germline (*spo-11; syp-1* heat stress bin 5=14.9 ± SD11.9; *spo-11; syp-1* no heat stress bin5=0.1 ± SD0.3; bin 5 $p<0.00001$, Mann Whitney) (Figure 8B). These results suggest that even in the absence of the SC, males experience a significant increase in SPO-11 independent DNA damage following heat stress.

Upon comparing the quantifications of the RAD-51 foci per nucleus between the *spo-11* heat stressed males and the *spo-11; syp-1* heat stressed males, I was surprised to find that *spo-11; syp-1* double mutant males displayed lower levels of DNA damage following heat stress compared with *spo-11* males (Figure 8B). In fact, this reduction in DNA damage was significant throughout the normalized germline ($p<0.00001$ for all bins, Mann Whitney) (Figure 8). This result was unexpected, as it indicates that loss of the SC might suppress a subset of the heat-induced DNA damage in spermatocytes.

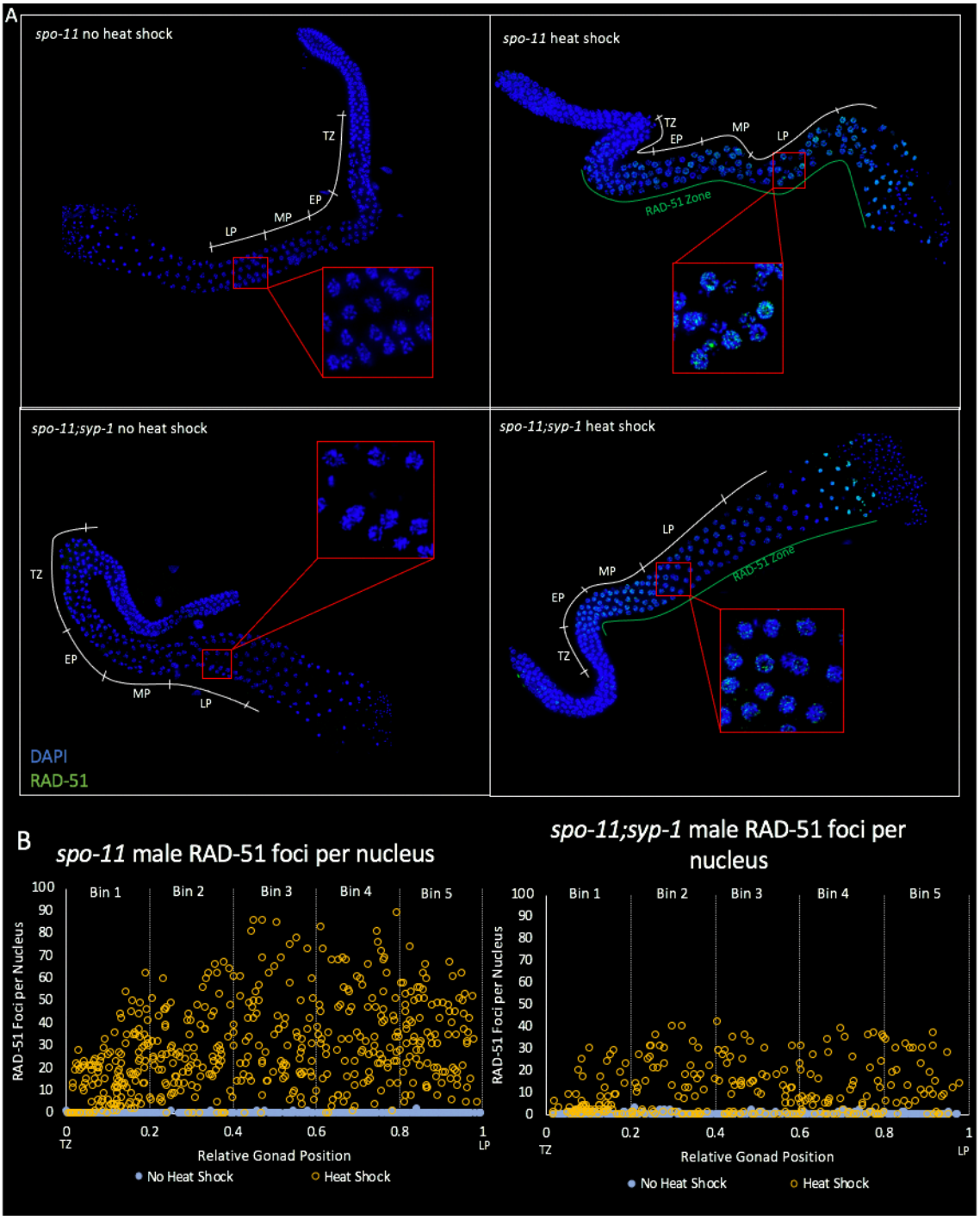

Figure 8: A loss of the SC suppresses heat-induced DNA damage in spermatocytes

(A)Immunofluorescence images of whole gonads featuring recombinase RAD-51 marking sites of DNA damage (green) and DAPI marking the DNA (blue). Windows featuring a zoomed in view to late pachytene are boxed in red. Images of *spo-11* null males and *spo-11; syp-1* double mutant males both with and without heat shock are included. The RAD-51 zone is marked by a solid green line. The stages of meiotic prophase I are marked with a white line.

(B) Scatterplots illustrating the quantification of RAD-51 foci per nucleus. The x axis represents the normalized length of the germline with 0 representing the beginning the of the transition zone and 1 representing the end of late pachytene. The y axis is the number of RAD-51 foci per nucleus, ranging from 0 foci to 100 foci. Data from the no heat shock group is represented by the solid blue dots, while data from the heat shock group is represented by the open yellow dots. *spo-11* null males are represented by the scatterplot to the left and *spo-11; syp-1* males are represented by the scatterplot to the left. *spo-11* male no HS: n=3, *spo-11* male HS: n=5, *spo-11; syp-1* male no HS: n=3, *spo-11; syp-1* male HS: n=3.

Average RAD-51 foci per nucleus of *spo-11* no heat stress males: bin 1=0.0±SD0.1, bin 2=0.0±SD0.2, bin 3=0.1±SD0.3, bin 4=0.0±SD0.1, bin 5=0.1±SD0.3. Average RAD-51 foci per nucleus of *spo-11* heat stress males: bin 1=17.2±SD13.6, bin 2=26.3±SD17.2, bin 3=34.4±SD21.6, bin 4=35.0±SD21.7, bin 5=34.2±SD17.2. Average RAD-51 foci per nucleus of *spo-11; syp-1* no heat stress males: bin 1=0.2±SD0.5, bin 2=0.2±SD0.6, bin 3=0.1±SD0.4, bin 4=0.2±SD0.5, bin 5=0.1±SD0.3. Average RAD-51 foci per nucleus of *spo-11; syp-1* heat stress males: bin 1=6.1±SD8.0, bin 2=12.4±SD12.5, bin 3=12.1±SD11.4, bin 4=10.7±SD12, bin 5=14.9±SD11.9.

Discussion

Evidence of a sexually dimorphic role of the SC during heat stress

Using *syp-1* and *spo-11; syp-1* mutants, I uncovered a novel sexually dimorphic role for the SC in the regulation of heat-induced DNA damage. I found that in the absence of the SC, heat-induced DNA damage was suppressed in males and increased in hermaphrodites. These findings reject my original hypothesis that loss of the SC would increase heat-induced DNA damage similarly for both sexes. Instead, these conclusions present a much more interesting story for SC dynamics during heat stress and potentially reveal the sexually dimorphic nature of the SC in *C. elegans*.

Presence of the SC might contribute to heat-induced DNA damage in males

Transposons are more active during heat stress in males

Transposons, or transposable elements (TEs), are segments of DNA that are capable of moving through the genome by either a "cut and paste" or "copy and paste" process (Ryan et al. 2016). When a TE moves in the genome it causes DNA damage because the excision of the TE leaves a DSB that must be repaired by the cell (Bessereau 2006). The germline is incredibly efficient at silencing this TE activity to ensure that an intact genome is transferred to the next generation (Sijen & Plasterk 2003). However, the Libuda Lab has found that upon heat stress, *C. elegans* spermatocytes display elevated levels of DNA damage that is caused by increased transposon activity and not the normal meiotic SPO-11 induced DSBs (Kurhanewicz et al. 2020). Additionally, the mammalian male germline relaxes transposon silencing at the onset of meiosis (van der Heijden & Bortvin 2009). Thus, a conserved feature of

spermatogenesis may be poor regulation of TEs raising the possibility of conserved sexually dimorphic features during meiosis that enable sex-specific silencing of TEs in the germline.

Interestingly, there is also evidence that demonstrates a relationship between TEs and the SC in multiple organisms. In rats, a majority of the DNA sequences associated with the lateral elements of the SC come from transposon-derived repeats (Hernández-Hernández et al. 2007). Additionally, in mice, SC-associated DNA contains segments with more than 80% homology to long and short interspersed repeated elements, which are characteristic of transposons (Pearlman et al. 1992). The theory behind positioning the TEs in the lateral elements is to prevent these sequences from engaging in DNA repair since SPO-11 induced DSBs do not occur within the sequences at the lateral elements (Hernández-Hernández et al. 2007). Further, these genomic regions that TEs typically associate with are highly repetitive regions and homologous recombination within repetitive DNA can lead to deletions and duplications (Piazza & Heyer 2019). While the changes in RAD-51 foci that I observed in *spo-11; syp-1* mutants have not been directly linked to changes in TE movement, it is intriguing to postulate that the SC may be influencing the movement of TEs in worms.

The SC is potentially involved with heat-induced DNA damage in spermatocytes

The increased levels of DNA damage that spermatocytes experience during heat stress may be causing the premature breakdown of the SC. One previous study linked elevated levels of exogenous DNA damage from irradiation with premature disassembly of the SC in late pachytene (Couteau & Zetka, 2011). This study only looked at hermaphrodites, therefore, it is unknown whether irradiation in males would cause a

similar SC breakdown. If males respond like hermaphrodites and prematurely lose the SC following irradiation, then it is possible that cells intentionally cause this break down to facilitate DNA repair. Indeed, in hermaphrodites it has been shown that DNA damage repair proteins may instigate this premature SC disassembly when there are high levels of exogenous DNA damage (Couteau & Zetka 2011). Thus, removal of the SC may alleviate restrictions on DNA damage repair and could explain why cells disassemble the complex

The suppression of the heat-induced DNA damage in *spo-11; syp-1* double mutant spermatocytes suggests that a subset of the heat-induced DSBs is dependent on presence of the SC. Nonetheless, there could be two or more DNA damage repair pathways occurring following heat-stress in spermatocytes. Homologous recombination is only one of the many DNA damage repair pathways that occur within cells. Homologous recombination is primarily used to repair DSBs during meiosis with other DNA damage repair pathways being actively suppressed (Ranjha et al., 2018). Additionally, homologous recombination requires the SC to repair DSBs, either SPO-11 induced or exogenously induced, with the homologous chromosome (Dernburg et al. 1998). Therefore, the subset of heat-induced DSBs that are dependent on the presence of the SC are those destined to be repaired by homologous recombination.

Under stressed conditions, it is possible that additional alternative DNA damage repair pathways can be activated and used during meiosis. These repair pathways include nonhomologous end joining (NHEJ), single-strand annealing (SSA), synthesis-dependent strand annealing (SDSA), and repair with the sister chromatid and there is evidence that all of these pathways can be accessed during hermaphrodite meiosis

(Chang et al. 2017, Ranjha et al. 2018, Toraason et al. 2021). All of these pathways do not load RAD-51 and instead use a different set of proteins to engage in DNA repair. Therefore, the heat-induced DSBs that appear to be suppressed based on RAD-51 staining in *spo-11; syp-1* spermatocytes may still be formed but are not undergoing homologous recombination and thus do not load RAD-51. These DSBs may be repaired using one of the alternative DNA repair pathways. Indeed, the Libuda lab has evidence that these alternative repair pathways are involved in the heat-induced DSBs in wild type spermatocytes. Future studies examining DNA repair within these *spo-11; syp-1* mutants may reveal a roll for the SC in constraining DSB repair to the homolog and a loss of the SC alleviates this restriction allowing for break repair with one of the alternative repair pathways. Further, the heat-induced DSBs that persist in *spo-11; syp-1* mutants may strictly rely on homologous repair mechanisms, which are unable to be repaired without the SC, contributing to the known fertility defects observed following heat stress (Kurhanewicz et al. 2021)

The SC may be restricting DNA damage repair in part through the highly organized DNA during meiosis (Hernández-Hernández et al. 2009). This chromatin/SC structure may present a barrier restricting the access of these alternative repair pathways to the DSBs (Zhu & Wani 2010). In budding yeast, SPO-11 induced DSBs are recruited to the SC for repair with the homolog (Keeney 2014, Hunter 2007). While it is unclear if heat-induced DSBs undergo this same recruitment to the SC, it is possible that a subset of these heat-induced DSBs might be confined by the SC and restricted to homologous recombination for repair similar to how SPO-11 DSBs are regulated. Therefore, spermatocytes upon exposure to elevated temperatures might intentionally

breakdown the SC to make the chromatin and DSBs more accessible to multiple DNA damage repair pathways for repair.

The SC may have a protective role against heat-induced DNA damage in hermaphrodites

In contrast to spermatocytes, a loss of the SC caused an increase in DBSs following heat stress in oocytes suggesting that the SC may have a protective role in late pachytene. Research within other organisms have demonstrated a role for the SC in suppressing damage to the genome. Notably, the SC has been implicated in flies in having a protective role against TE movement (Miller et al. 2020). While the SC is known to have a conserved function across different organisms, the genes that make up the SC actually hold little sequence homology outside of the genus; this indicates that the genes of the SC are rapidly evolving across species (Hemmer & Blumenstiel 2016, Fraune et al. 2013). In flies it is postulated that this rapid sequence evolution of SC genes may facilitate the ability of the SC to suppress TE movement during meiosis. (Miller et al. 2020)

Currently, *C. elegans* hermaphrodites displayed no evidence of TE mobilization upon heat shock in worms, and it is unknown if a loss of the SC enables TE mobilization following heat stress (Kurhanewicz et al., 2020). Future studies looking at the movement of TEs in hermaphrodite worms following the loss of the SC could reveal a direct relationship between the SC and TEs in hermaphrodites.

Sexual differences in SC structure

Multiple studies in many organisms have suggested the SC may display sexually dimorphic features and these features might contribute to the hermaphrodite-specific protective role of the SC (Agostinho et al. 2018, von Wettstein et al. 1984). There are many potential mechanisms through which the SC may avoid premature disassembly in heat-shocked hermaphrodites. The hermaphrodite SC may interact with other proteins that contribute to its stability during heat stress. Alternatively, the hermaphrodite SC may undergo sex-specific post-translational modifications that prevent it from disassembling prematurely as the male SC does during heat stress. The SC is known to be both phosphorylated and SUMOylated in many organisms with these modifications being important for the assembly, disassembly, and function of the complex during meiosis (Cheng et al. 2006, Gao et al. 2016, Gao & Colaiácovo 2018). Both of these modifications may cause the structure of the SC to be different between the sexes contributing to the stability differences during heat stress.

Additionally, there is evidence of sex-specific structural differences in the SC in other organisms. For example, in mice it was found that the width between the lateral elements of the SC is about 60 nm shorter in females than in males (Agostinho et al. 2018). A similar discrepancy is seen in the silkworm, where the females have a width between the lateral elements that is about 30-40 nm shorter than in males (von Wettstein et al. 1984). The width of the SC is just one feature that may be structurally different between males and hermaphrodites. It is unknown currently if there are any structural differences between spermatocyte and oocyte SCs, but additional studies using electron microscopy could help to answer this question. Future studies investigating the SC

structure in both sexes may reveal these differences both using high resolution microscopy and examining post-translational modifications.

Notably, my data reveals that like in other organisms, SC mutants in *C. elegans* behave differently across the sexes. *syp-1* mutants in no heat stress conditions displayed nearly opposite patterns of DNA damage with hermaphrodites exhibiting higher RAD-51 levels that increase progressively through late pachytene and males exhibiting a drop off in RAD-51 foci during pachytene (Figures 5, 7). Thus, the SC appears to behave differently in hermaphrodites versus males in both normal and heat stress conditions. If structural differences do exist between spermatocytes and oocytes, then it may explain these behavioral differences of the SC.

Conclusion

My data demonstrates that the SC has sexually dimorphic characteristics in *C. elegans,* exhibiting opposite sex-specific roles during heat stress. Uncovering this aspect of the SC brings the field another step closer to understanding the mechanisms that underlie the heat-induced infertility that is specific to males. Infertility is much more than a simple physiological problem. It can have a vast impact on individuals and couples for whom the inability to reproduce creates psychological distress. In order to help prevent or treat this condition, it is essential that the field continues to learn more about the mechanisms that underlie male infertility. This study lays an initial foundation for understanding how the SC may be contributing to this sexually dimorphic response to heat exposure and thus to male infertility. The conclusions from my research may help to identify potential therapies and lifestyle changes that could mitigate the effects of male infertility.

Bibliography

Agostinho, A., Kouznetsova, A., Hernandez-Hernandez, A., Bernhem, K., Blom, H., Hoog, C. (2018). Sexual dimorphism in the width of the mouse synaptonemal complex. *J Cell Sci*, 131(5): jcs212548.

Baumann, P., West, S.C. (1998). Role of the human RAD51 protein in homologous recombination and double-stranded-break repair. *Trends Biochem Sci,* 23(7): 247-51.

Bessereau, J.L. (2006). Transposons in *C. elegans*. *Wormbook.*

Bhalla, N., Dernburg, A. F. (2005). A conserved checkpoint monitors meiotic chromosome synapsis in *Caenorhabditis elegans*. *Science*, *310*(5754):1683-1686.

Bilgir, C., Dombecki, C.R., Chen, P.F., Villenueve, A.M., Nabeshima, K. (2013). Assembly of the synaptonemal complex is a highly temperature-sensitive process that is supported by PGL-1 during *Caenorhabditis* elegans meiosis. *G3*, 3(4): 585-595.

Bohr, T., Guinevere, A., Eggleston, E., Firestone, K., Bhalla, N. (2016). Synaptonemal complex components are required for meiotic checkpoint function in *Caenorhabditis elegans*. *Genetics*, *204*(3):987-997.

Brenner, S. (1974). The genetics of *Caenorhabditis elegans*. *Genetics*, 77:71-94.

Cahoon, C.K., Hawley, R.S. (2016). Regulating the construction and demolition of the synaptonemal complex. *Nat Struct Mol Bio*, 23(5): 369-377.

Cahoon, C. K., Libuda, D.E. (2019). Leagues of their own: sexually dimorphic features of meiotic prophase I. *Chromosoma*, *128*:199-214.

Cahoon, C.K., Helm, J.M., Libuda, D.E. (2019). Synaptonemal complex central region proteins promote localization of pro-crossover factors to recombination events during *Caenorhabditis elegans* meiosis. *Genetics*, 213(2): 395-409.

Chang, H.H.Y., Pannunzio, N.R., Adachi, N., Lieber, M.R. (2017). Non-homologous end joining and alternative pathways to double-strand break repair. *Nature Review Molecular Cell Biology*, 18:495-506.

Cheng, C.H., Lo, Y.H., Liang, S.S., Ti, S.C., Lin, F.M., Yeh, C.H, Huang, H.Y., Wang, T.F. (2006). SUMO modifications control assembly of synaptonemal complex and polycomplex in meiosis of *Saccharomyces cerevisiae*. *Genes & Dev*, 20:2067-2081.

Clejan, I., Boerckel, J., Ahmed, S. (2006). Developmental modulation of nonhomologous end joining in *Caenorhabditis elegans*. *Genetics*, 173(3):1301-1317.

Colaiácovo, M.P., MacQueen, A.J., Martinez-Perez, E., McDonald, A., Adamo, A., La Volpe, A., Villeneuve, A.M. (2003). Synaptonemal complex assembly in *C. elegans* is dispensable for loading strand-exchange proteins but critical for proper completion of recombination. *Dev. Cell.*, 5:463-474.

Couteau, F., Zetka, M. (2011). DNA damage during meiosis induces chromatin remodeling and synaptonemal complex disassembly. *Developmental cell*, 20(3):353-363.

Dernburg, A. F., McDonald, K., Moulder, G., Barstead, R., Dresser, M., & Villeneuve, A. M. (1998). Meiotic recombination in C. elegans initiates by a conserved mechanism and is dispensable for homologous chromosome synapsis. *Cell*, *94*:387-398.

Fraune, J., Brochier-Armanet, C., Alsheimer, M., Benavente, R. (2013). Phylogenies of central element proteins reveal the dynamic evolutionary history of the mammalian synaptonemal complex: ancient and recent components. *Genetics*, 195(3):781-793.

Gao, J. Barroso, C., Kim, H.M., Li, S., Labrador, L., Lightfoot, J., et al. (2016). N-terminal acetylation promotes synaptonemal complex assembly in *C. elegans*. *Genes & Dev*, 30:2404-2416.

Gao, J., Colaiácovo, M.P. (2018). Zipping and unzipping: protein modifications regulating synaptonemal complex dynamics. *Trends in Genetics*, 34(3):232-245.

Hassold, T., Hunt, P. (2001). To err (meiotically) is human: the genesis of human aneuploidy. *Nat Rev Genet*, *2*(4):280-291.

Hemmer, L.W., Blumenstiel, J.P. (2016). Holding it together: rapid evolution and positive selection in the synaptonemal complex of *Drosophila*. *BMC Evolutionary Biology*, 16:91.

Hernández-Hernández, A., Rincón-Arano, H., Recillas-Targa, F., Ortiz, R., Valdes-Quezada, C., Echeverría, O.M., et al. (2007). Differential distribution and association of repeat DNA sequences in the lateral element of the synaptonemal complex in rat spermatocytes. *Chromosoma*, 117:77-87.

Hernández-Hernández, A., Vázques-Nin, G.H., Echeverría, O.M., Recillas-Targa, F. (2009). Chromatin structure contribution to the synaptonemal complex formation. *Cellular Molecular Life Sciences*, 66:1198-1208.

Hillers, K.J., Jantsch, V., Martinez-Perez, E., Yanowitz, J.L. (2017). Meiosis. *Wormbook*.

Huelgas-Morales, G., Greenstein, D. (2018). Control of oocyte meiotic maturation in C. elegans. *Seminars in Cell & Developmental Biology*, *84*:90-99.

Hunter, N. (2007). Meiotic recombination. *Molecular Genetics of Recombination. Topics in Current Genetics,* 17.

Hunter, N. (2015). Meiotic Recombination: The Essence of Heredity. *Cold Spring Harbor perspectives in biology*, *7*(12).

Hurlock, M.E., Cavka, I., Kursel, L.E., Haversat, J., Wooten, M., Nizami, Z., et al. (2020). Identification of novel synaptonemal complex components in *C. elegans*. *Journal of Cell Biology*, 219(5):e201910043.

Jaramillo-Lambert, A., Ellefson, M., Villeneuve, A. M., Engebrecht, J. (2007). Differential timing of S phases, X chromosome replication, and meiotic prophase in the C. elegans germ line. *Dev Biology*, *308*(1):206-221.

Keeney, S., Giroux C.N., Kleckner, N. (1997). Meiosis-specific DNA double0stran breaks are catalyzed by Spo11, a member of a widely conserved protein family. *Cell*, 88(3):375-384.

Keeney, S., Lange, J., Mohibullah, N. (2014). Self-organization of meiotic recombination initiation: general principles and molecular pathways. *Annual Review of Genetics*, 48(1):187-214.

Kim, B., Park, K., Rhee, K. (2013). Heat stress response of male germ cells. *Cell Mol Life Sci*, *70*(15):2623-2636.

Kurhanewicz, N. A., Dinwiddie, D., Bush, Z. D., Libuda, D. E. (2020). Elevated temperatures cause transposon-associated DNA damage in C. elegans spermatocytes. *Current Biology*, *S0960-9822*(20):31420-2.

Lai, C. H., Chou, C. Y., Ch'ang, L. Y., C., Liu, C. S., Lin, W. (2000). Identification of novel human genes evolutionarily conserved in Caenorhabditis elegans by comparative proteomics. *Genome Res*, *10*(5):703-713.

Lemmens, B.B.L.G., Tijsterman, M. (2011). DNA double-strand break repair in Caenorhabditis elegans. *Chromosoma*, *120*(1):1-21.

Libuda, D. E., Uzawa, S., Meyer, B. J., Villeneuve, A. M. (2013). Meiotic chromosome structures constrain and respond to designation of crossover sites. *Nature*, *502*(7473):703-706.

Lui, D. Y., Colaiacovo, M. P. (2013). Meiotic development in Caenorhabditis elegans. *Adv Exp Med Biol.*, *757*:133-170.

MacQueen, A. J., Colaiacovo, M. P., McDonald, K., Villeneuve, A. M. (2002). Synapsis-dependent and -independent mechanisms stabilize homolog pairing during meiotic prophase in C. elegans. *Genes & development.*, *16*:2428-2442.

Martin, R. H. (2008). Meiotic errors in human oogenesis and spermatogenesis. Reprod Biomed Online, 16(4):523-31.

Miller, D.E. (2020) Synaptonemal Complex-Deficient Drosophila melanogaster Females Exhibit Rare DSB Repair Events, Recurrent Copy-Number Variation, and an Increased Rate of de Novo Transposable Element Movement. *G3*, 10(2), 525-527.

Morelli, M. A., Cohen, P. E. (2005). Not all germ cells are created equal: aspects of sexual dimorphism in mammalian meiosis. *Reproduction*, *130*(6):761-781.

Morgan, C. H., Zhang, H., Bomblies, K. (2017). Are the effects of elevated temperature on meiotic recombination and thermotolerance linked via the axis and synaptonemal complex? *Philos Trans R Soc Lond Ser B Biol Sci*, *372*(1736):20160470.

Murakami, H., Keeney, S. (2008). Regulating the formation of DNA double-strand breaks in meiosis. *Genes & development*, *22*(3):286-292.

Nagaoka, S. I., Hassold, T. J., Hunt, P. A. (2012). Human aneuploidy: mechanisms and new insights into an age-old problem. *Nature Reviews: Genetics*, *13*:493-504.

Page, S. L., Hawley, R. S. (2003). Chromosome choreography: the meiotic ballet. *Science*, *301*:785-789.

Page, S.L., Hawley, R.S. (2004). The genetics and molecular biology of the synaptonemal complex. *Annual Review of Cell and Developmental Biology*, 20:525-558.

Pattabiraman, D., Roelens, B., Woglar, A., Villeneuve, A. M. (2017). Meiotic recombination modulates the structure and dynamics of the synaptonemal complex during C. elegans meiosis. *PLOS Genetics*.

Pearlman, R.E., Tsao, N., Moens, P.B. (1992). Synaptonemal complexes from Dnase-treated rat pachytene chromosomes contain (Gt)(n) and line/sine sequences. *Genetics*, 130(4): 865-872

Perez-Crespo, M., Pintado, B., Guitierrez-Adan, A. (2008). Scrotal heat stress effects on sperm viability, sperm DNA integrity, and the offspring sex ratio in mice. *Mol Reprod Dev*, *75*(1):40-47.

Phillips, C. M., Meng, X., Zhang, L., Chretien, J. H., Urnov, F. D., Dernburg, A. F. (2009). Identification of chromosome sequence motifs that mediate meiotic pairing and synapsis in C. elegans. *Nat Cell Bio*, *11*(8):943-942.

Piazza, A., Heyer, W.D. (2019). Homologous recombination and the formation of complex genomic rearrangements. *Trends in Cell Biology*, 29(2):135-149.

Preibisch, S., Saalfeld, S., Tomancak, P. (2009). Globally optimal stitching of tiled 3D microscopic image acquisitions. *Bioinformatics*, 25(11):1463-1465.

Ranjha, L., Howard, S. M., Cejka, P. (2018). Main steps in DNA double-strand break repair: an introduction to homologous recombination and related processes. *Chromosoma*, *127*:187-214.

Rao, M., Zhao, X.L., Yang, J., Hu, S.F., Lei, H., Xia, W., Zhu, C.H. (2015). Effect of transient scrotal hyperthermia on sperm parameters, seminal plasma biochemical markers, and oxidative stress in men. *Asian J Androl.,* 17(4):668-75.

Roeder, G.S. (1997). Meiotic chromosomes: it takes two to tango. *Genes & Dev*, 11:2600-2621.

Ryan, C. P., Brownlie, J. C., Whyard, S. (2016). Hsp90 and physiological stress are linked to autonomous transposon mobility and heritable genetic changes in nematodes. *Genome Biol Evol*, *8*(12):3794-3805.

Schlegel, P. N. (2009). Evaluation of male infertility. *Minerva Ginecol.*, *61*(4), 261-83.

Shakes, D. C., Wu, J., Sadler, P. L., LaPrade, K., Moore, L. L., Noritake, A., Chu, D. S. (2009). Spermatogenesis-specific features of the meiotic program in Caenorhabditis elegans. *PloS Genet*, *5*(8):e1000611.

Sijen, T., Plasterk, R.H.A. (2003). Transposon silencing in the *Caenorhabditis elegans* germline by natural RNAi. *Nature*, 426:310-314.

Smolikov, S., Eizinger, A., Schild-Prufert, K., Hurlburt, A., McDonald, K., Engebrecht, J., Villeneuve, A.M., Colaiácovo, M.P. (2007). SYP-3 restricts synaptonemal complex assembly to bridge paired chromosome axes during meiosis in *Caenorhabditis elegans*. *Genetics*, 176(4):2015-2025.

Toraason, E., Adler, V.L., Kurhanewicz, N.A., DiNardo, A., Saunders, A.M., Cahoon, C.K., Libuda, D.E. (2021). Automated and customizable quantitative image analysis of whole *C. elegans* germlines. *Genetics*, 217(3):iyab010.

van der Heijden, G. W., Bortvin, A. (2009). Transient relaxation of transposon silencing at the onset of mammalian meiosis. *Epigenetics*, *4*(2):76-79.

von Wettstein, D., Rasmussen, S. W., Holm, P. B. (1984). The synaptonemal complex in genetic segregation. *Annu Rev Genet*, *18*:331-413.

Villeneuve, A. (1994). A cis-acting locus that promotes crossing over between X chromosomes in *Caenorhabditis elegans*. *Genetics*, *136*(3):887-902.

Wang, Y., et al. (2019). Reprogramming of meiotic chromatin architecture during spermatogenesis. *Mol Cell*, *73*(3):547-561.

Yang, F., De La Fuenta, R., Leu, N.A., Baumann, C., McLaughling, K.J., Wang, P.J. (2006). Mouse SYCP2 is required for synaptonemal complex assembly and chromosomal synapsis during male meiosis. *J Cell Bio*, 173(4):497-507.

Yang, F., Eckardt, S., Leu, N. A., McLaughlin, K. J., Wang, P. J. (2008). Mouse TEX15 is essential for DNA double-strand break repair and chromosomal synapsis during male meiosis. *J Cell Biol*, *180*(4):673-679.

Yeh, H., Lin, S., Wu, Y., Chan, N., Chi, P. (2017). Functional characterization of the meiosis-specific DNA double-strand break inducing factor SPO-11 from C. elegans. *Sci Rep*, *7*(2370).

Yuan, L., Liu, J. G., Zhao, J., Brundell, E., Daneholt, B., Hoog, C. (2000). The murine SCP3 gene is required for synaptonemal complex assembly, chromosome synapsis, and male fertility. *Mol Cel*, *5*(1):73-83.

Zhu, Q., Wani, A. A. (2010). Histone modifications: crucial elements for damage response and chromatin restoration. *J Cell Physiol*, *223*(2):283-288.

Zarkower, D. (2006) Somatic sex determination. *Wormbook*.